

A Robust Scheme for PSS Detection and Integer Frequency Offset Recovery in LTE Systems

Michele Morelli, *Senior Member, IEEE*, and Marco Moretti, *Member, IEEE*

Abstract—Before establishing a communication link in a cellular network, the user terminal must activate a synchronization procedure called initial cell search in order to acquire specific information about the serving base station. To accomplish this task, the primary synchronization signal (PSS) and secondary synchronization signal (SSS) are periodically transmitted in the downlink of a Long Term Evolution (LTE) network.

Since SSS detection can be performed only after successful identification of the primary signal, in this work we present a robust scheme for joint PSS detection, sector index identification and integer frequency offset (IFO) recovery in an LTE system. The proposed algorithm relies on the maximum likelihood (ML) estimation criterion and exploits a suitable reduced-rank representation of the channel frequency response to take multipath distortions into account. We show that some PSS detection methods that were originally introduced through heuristic reasoning can be derived from our ML framework by selecting an appropriate model for the channel gains over the PSS subcarriers.

Numerical simulations indicate that the proposed scheme can be effectively applied in the presence of severe multipath propagation, where existing alternatives provide unsatisfactory performance.

Index Terms—LTE, cell search, sector index identification, integer frequency offset recovery.

I. INTRODUCTION

The Long Term Evolution (LTE) mobile communication standard has been developed by the 3rd Generation Partnership Project (3GPP) in order to enhance the performance of currently deployed 3G systems in terms of data throughput, spectrum utilization and user mobility [1]. This technology supports various channel bandwidths ranging from 1.4 to 20 MHz and promises peak data rates of 100 Mbit/s in the downlink (DL) and 50 Mbit/s in the uplink (UL) for the 20 MHz system bandwidth [2]. Improved resilience against multipath distortion, high spectral efficiency and ability to handle different data rates are achieved by using orthogonal frequency-division multiple-access (OFDMA) in the DL, while single-carrier frequency-division multiple-access (SC-FDMA) is adopted in the UL due to its reduced peak-to-average power-ratio [3]. There is also the possibility of choosing between normal and extended cyclic prefix (CP), the latter being considered for large delay spread environments.

LTE supports multi-cell communications, with cell information being conveyed by an integer number called cell-ID. Upon entering the network or during an handover operation, the user equipment (UE) must recover the cell-ID of the serving base station (eNodeB) and has also to acquire correct timing

and frequency synchronization. This operation is known as initial *cell-search* [4], [5] and is accomplished by exploiting a dedicated synchronization channel (SCH) periodically inserted in the DL radio frame [6]. The SCH conveys two signals called Primary Synchronization Sequence (PSS) and Secondary Synchronization Sequence (SSS). The former is generated from a 63-length frequency-domain Zadoff-Chu (ZC) sequence whose root index univocally determines the sector identity. The latter is an interleaved concatenation of two length-31 scrambled m -sequences specifying the cell ID group.

Although in principle it is possible to consider the joint estimation of all synchronization parameters and cell-ID, a more pragmatic approach relies on the following three-stage procedure [7]:

- 1) Firstly, fractional frequency offset (FFO) and coarse symbol timing recovery is accomplished using the redundancy introduced by the CP. This method was originally proposed in [8] and its accuracy can be improved by averaging the timing and frequency metrics over several OFDM symbols;
- 2) In the second step, the UE detects the position of the PSS within the received DL signal in order to acquire subframe timing information, and also determines the sector index by identifying which primary sequence has been transmitted out of three possible alternatives. The integer frequency offset (IFO) can be retrieved at this stage by evaluating the shift of the received PSS in the frequency domain;
- 3) The final step recovers the cell ID group and identifies the frame boundary by using the received SSS. Once these operations have been completed, the UE is able to read some basic configuration information broadcast from the eNodeB, such as the system bandwidth, CP length and duplexing mode.

Since SSS detection can be accomplished only after successful identification of the primary sequence, PSS detection represents a crucial task in the overall cell search procedure. For this reason, it has attracted much attention in the last few years and many solutions are currently available. Some of them operate in the time-domain (TD), while others exploit the frequency-domain (FD) samples provided by the receive discrete Fourier transform (DFT) unit. Examples of TD schemes can be found in [9]-[11], where the PSS is revealed by looking for the peak of the cross-correlation between the received samples and the three locally regenerated ZC sequences. However, since the SCH is transmitted onto a set of 62 dedicated subcarriers with the other subcarriers being modulated by data symbols, the PSS should be extracted from

M. Morelli and M. Moretti are with the University of Pisa, Dipartimento di Ingegneria dell'Informazione, Italy. Email: {michele.morelli, marco.moretti}@iet.unipi.it.

the DL signal before the correlation stage. This requires a high-order filtering operation of the received signal, which results into an increase of the hardware complexity and also leads to some performance degradation since the contribution of data subcarriers cannot be totally filtered out due to the spectral leakage and the uncompensated CFO. TD methods with reduced complexity are suggested in [12] and [13], where the tasks of PSS detection and sector index recovery are decoupled by either exploiting the central symmetric-property of the ZC sequences or by correlating the DL signal with the sum of the three possible primary sequences.

As an alternative to the TD approach, in FD schemes the contribution of the data-bearing subcarriers is eliminated by selecting the SCH at the receive DFT output and correlating the resulting samples with replicas of the three tentative frequency-domain ZC sequences [14]. This method works properly as long as the channel gain can be considered as approximately constant over the SCH subband. Unfortunately, such an assumption does not hold for transmissions over severe multipath channels or in the presence of a non-negligible timing error, which appears as a linearly increasing phase shift at the DFT output. In these circumstances, the correlation properties of the received PSS will be irreparably destroyed with an ensuing degradation of the system performance. To solve this problem, differential correlation in the FD has been proposed in [15], where IFO detection is also accomplished during the PSS match process. A disadvantage of the differential approach is that the peaks of the resulting metric are quite close for different IFO values, thereby reducing its ability to recover the frequency error [16]. Furthermore, compared to [14], the accuracy of the FD differential correlator is greatly reduced whenever the channel frequency response (CFR) over the SCH is approximately constant. For this reason, the authors of [17] propose to adaptively choose between non-differential and differential detection on the basis of a previous estimate of the maximum channel delay spread. A simpler solution is found in [18] by resorting to the partial correlation concept, wherein the received SCH is partitioned into several adjacent FD segments which are subsequently correlated with the corresponding parts of the tentative ZC sequences. A fundamental design parameter of this approach is represented by the number of segments, which must be selected in accordance with the coherence bandwidth of the transmission channel.

It is worth noting that all the aforementioned methods have been derived by means of heuristic reasoning. In order to check whether their performance can be substantially improved or not, it is of interest to make comparisons with alternative approaches based on some optimality criterion. With this goal in mind, in the present work we employ maximum likelihood (ML) methods to study the problem of PSS detection, sector index identification and IFO recovery, which represents the second step of the cell search process in an LTE system. In contrast to previous investigations, our analysis, which originates from the work presented in [19], explicitly takes into account the multipath distortion introduced by the propagation medium on the received signal. This is achieved by treating the CFR over the SCH subcarriers as a nuisance vector [20], which is jointly estimated along with the synchronization

parameters. As we shall see, this approach may lead to an under-determined estimation problem wherein the number of quantities to be recovered exceeds the number of available data. Reduced-rank approximations of the CFR are proposed to cope with such a situation using either the minimum mean square-error criterion (MMSE) or the classical polynomial basis expansion. This approach results into a general framework which includes both the conventional FD scheme [14] and the partial correlation concept [18] through a suitable selection of the CFR model. A key assumption of our analysis is that symbol timing and FFO have been previously acquired using the classical CP-based method presented in [8]. However, since multipath propagation may significantly reduce the accuracy of the timing estimates provided by [8], a residual timing error is included in the adopted system model and numerical simulations are used to assess its impact on the overall performance.

The rest of the paper is organized as follows. Next section illustrates the signal model and formulates the estimation problem. Sect. III presents the joint ML estimator of the unknown parameters using a generic expansion basis to represent the CFR. An MMSE reduced-rank approximation of the CFR is derived in Sect. IV along with other possible channel representations that lead to alternative known PSS detection schemes. After discussing numerical simulations in Sect. V, we offer some conclusions in Sect. VI.

Notation: Matrices and vectors are denoted by boldface letters, with \mathbf{I}_N being the identity matrix of order N , $\mathbf{0}_K$ the K -dimensional null vector and $\mathbf{1}_K$ a K -dimensional vector with unit entries. The notation $\|\cdot\|$ indicates the norm of the enclosed vector, while \mathbf{B}^{-1} and $\text{tr}\{\mathbf{B}\}$ are the inverse and the trace of a matrix \mathbf{B} . We use $\mathbb{E}\{\cdot\}$, $(\cdot)^*$, $(\cdot)^T$ and $(\cdot)^H$ for expectation, complex conjugation, transposition and Hermitian transposition, respectively. The notation $\Re\{\cdot\}$ stands for the real part of a complex-valued quantity, while $|\cdot|$ represents the corresponding modulus. Finally, we use $\hat{\lambda}$ to indicate a trial value of an unknown parameter λ .

II. SYSTEM MODEL

A. LTE frame structure

We consider the DL of an LTE system operating in frequency-division-duplexing (FDD) mode. As shown in Fig. 1, data transmission is organized in radio frame units of length 10 ms. Each frame is divided into ten 1 ms subframes, which are further partitioned into two slots of length 0.5 ms. Every slot contains 7 OFDMA symbols in case of normal CP, while 6 OFDMA symbols are present when the extended CP is employed to cope with a large delay spread. In the time-frequency grid, system resources are divided into resource blocks (RBs), such that each RB is composed of 12 contiguous subcarriers for a duration of one slot. According to the LTE specifications, 504 different physical-layer cell IDs are available and arranged into 168 distinct groups. Each group is identified by the cell ID group $N_{ID}^{(1)} \in \{0, 1, \dots, 167\}$ and contains three different sectors, which are specified by the sector ID $N_{ID}^{(2)} \in \{0, 1, 2\}$. In addition to acquiring the correct timing and frequency synchronization, during the cell search

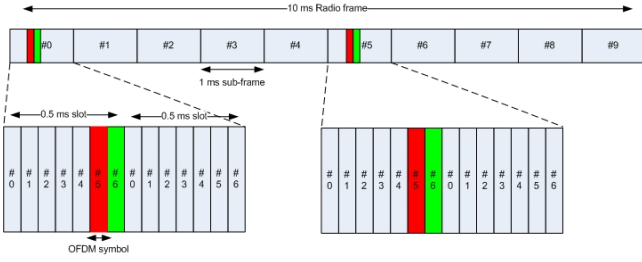


Fig. 1. Position of PSS (green) and SSS (red) in the LTE downlink frame.

procedure the UE must retrieve the integer-valued parameters $N_{ID}^{(1)}$ and $N_{ID}^{(2)}$, from which the cell ID of the serving eNodeB is uniquely computed as $N_{ID}^{cell} = 3N_{ID}^{(1)} + N_{ID}^{(2)}$. To accomplish these tasks, two synchronization sequences called PSS and SSS are periodically transmitted on a dedicated SCH to specify the sector ID and cell group, respectively. In particular, the PSS is located in the last OFDM symbol of the first and 11th slots of each radio frame, while the SSS is transmitted in the symbol immediately preceding the PSS. As LTE allows for various system bandwidths, both PSS and SSS are mapped onto a 73-subcarriers subband located symmetrically around DC, which corresponds to the smallest allowable spectrum occupancy. Such design choice enables the detection of the synchronization signals without requiring explicit knowledge of the system bandwidth.

B. Primary synchronization sequence

The PSS is chosen in a set of three different 63-length ZC sequences characterized by excellent auto- and cross-correlation properties [21]. More precisely, during the PSS transmission the SCH subcarriers with indices $n \in \{0, \pm 1, \pm 2, \dots, \pm 36\}$ are modulated by the following polyphase complex exponential terms

$$a_u(n) = \begin{cases} e^{-j\pi u(n^2 + 63n + 110)/63} & \text{if } n \in \mathcal{I} \\ 0 & \text{otherwise} \end{cases} \quad (1)$$

where u denotes the root index of the selected ZC sequence and $\mathcal{I} = \{n \in \mathbb{Z} : |n| \leq 31 \text{ and } n \neq 0\}$. The above equation indicates that, out of the 73 available subcarriers, only 62 are modulated by the PSS, while the remaining eleven (five placed at the SCH boundaries and one placed at DC) are left unfilled. The root index belongs to the set $\mathcal{J}_u = \{25, 29, 34\}$ and specifies the sector ID $N_{ID}^{(2)}$ as shown in Table I.

TABLE I
RELATIONSHIP BETWEEN $N_{ID}^{(2)}$ AND ZC ROOTS

$N_{ID}^{(2)}$	Root index u
0	25
1	29
2	34

C. Overview of the cell search procedure

Cell search is a three-stage procedure which is performed when the UE is switched on or when it loses synchronization.

Since LTE must provide mobility up to 350 km/h, this process is periodically repeated to find a candidate cell for the handover operation. In the first stage, the UE retrieves the FFO and acquires coarse information about the OFDM symbol timing. This operation is typically accomplished in the time domain using the conventional CP-based delay correlation method presented in [8]. After FFO correction and CP removal, the resulting samples are converted in the frequency domain using a DFT unit. The second stage detects the position of the PSS within the received DL signal and recovers the ZC root index u . These tasks can be accomplished either in the time or frequency domain, and provide subframe timing information as well as the sector ID. In the third stage, the SSS is exploited to get the cell ID group and the frame boundary. Recalling that the SSS is located in the symbol immediately preceding the PSS, the latter is normally used as a phase reference to perform coherent detection of the SSS in the frequency domain. As for the IFO, it can be estimated either in the second or third step by evaluating the frequency domain shift of the received PSS or SSS at the DFT output. However, since there are 168 different secondary sequences compared to only three primary sequences, the complexity of the IFO search is greatly reduced if it is performed in the second step in conjunction with PSS detection.

D. Signal model and problem formulation

We now concentrate on the second stage of the cell search process and provide the signal model for PSS detection and IFO recovery. The DL signal propagates through a multipath channel with discrete-time impulse response $\mathbf{h} = [h(0), h(1), \dots, h(L-1)]^T$ of order L . At the UE receiver, the incoming signal is down-converted to baseband and sampled with period T_s . Then, the CP delay correlation method [8] is applied to retrieve the FFO and the OFDM symbol timing. After FFO compensation, timing information is exploited to remove the CP and to divide the stream of time-domain samples into segments $\mathbf{x}_k = [x_k(0), x_k(1), \dots, x_k(N-1)]$ (with $k = 1, 2, \dots$) which are subsequently fed to the N -point DFT unit. We denote by

$$X_k(n) = \frac{1}{\sqrt{N}} \sum_{\ell=0}^{N-1} x_k(\ell) e^{-j2\pi \ell n/N} \quad (2)$$

the n th DFT output corresponding to the k th segment and assume that the accuracy of the frequency and timing estimates is such that we can reasonably neglect any inter-channel or inter-block interference present on $X_k(n)$. However, due to a possible residual timing error, the quantities $X_k(n)$ will be affected by a phase rotation that increases linearly with the subcarrier index n . Since the PSS is transmitted twice per frame, the observation window for PSS detection encompasses N_Q adjacent OFDM symbols composing a half frame, with N_Q being either 60 or 70 for the extended or normal CP transmission mode, respectively. Without loss of generality, in this work we consider an LTE system with an extended CP and let $N_Q = 60$. Furthermore, we assume that the PSS is transmitted on the q th OFDM symbol within the observation window $k = 1, 2, \dots, N_Q$ and denote by

$\mathbf{X}_k = [X_k(-36), X_k(-35), \dots, X_k(36)]$ the 73-dimensional vector collecting the DFT output over the SCH channel. Then, for $k \neq q$ we model \mathbf{X}_k as a zero mean Gaussian vector with covariance matrix $\mathbf{C}_k = \sigma_k^2 \mathbf{I}_{73}$ (σ_k^2 being an unknown parameter), while for $k = q$ we have

$$X_q(n) = H(n-\nu)a_u(n-\nu)e^{j2\pi(n-\nu)\theta/N} + w_q(n) \quad |n| \leq 36 \quad (3)$$

where ν represents the IFO, θ denotes the residual timing error (normalized by the sampling period) and $H(n)$ is the CFR over the n th subcarrier. Finally, $w_q(n)$ is the noise contribution, which is modeled as a circularly-symmetric white Gaussian process with average power $\sigma_w^2 = \mathbb{E}\{|w_q(n)|^2\}$. Without loss of generality, we consider θ as an integer-valued parameter. The reason is that any residual fractional timing offset (FTO) can be incorporated into $h(\ell)$ by letting $h(\ell) = h(t)|_{t=(\ell+\varepsilon)T_s}$, where ε denotes the FTO and $h(t)$ is the continuous-time version of the channel impulse response (CIR).

Our goal is to exploit the set of observations $\mathbf{X} = [\mathbf{X}_1^T \mathbf{X}_2^T \dots \mathbf{X}_{N_Q}^T]^T$ to find the joint ML estimate of the unknown parameters $\{q, u, \nu\}$ specifying the PSS position, the sector ID and the IFO. Unfortunately, this task is complicated by the presence of the nuisance quantities $\{\mathbf{H}, \theta, \sigma^2, \sigma_w^2\}$, where $\mathbf{H} = \{H(n); |n| \leq 31\}$ and $\sigma^2 = \{\sigma_k^2; 1 \leq k \leq N_Q \text{ and } k \neq q\}$. In order to reduce the number of estimation parameters, we propose to merge \mathbf{H} and θ into an equivalent CFR $\mathbf{H}_{eq} = \{H_{eq}(n); |n| \leq 31\}$ with elements $H_{eq}(n) = H(n)e^{-j2\pi n\theta/N}$. Moreover, since channel gains over blocks of contiguous subcarriers are highly correlated, we expect that \mathbf{H}_{eq} can be accurately expanded over a reduced-rank basis of $P < 63$ vectors $\{\mathbf{b}_1, \mathbf{b}_2, \dots, \mathbf{b}_P\}$. This amounts to putting

$$\mathbf{H}_{eq} \simeq \mathbf{B}\boldsymbol{\xi} \quad (4)$$

where \mathbf{B} is a matrix with columns \mathbf{b}_i ($i = 1, 2, \dots, P$) and $\boldsymbol{\xi} = [\xi(1), \xi(2), \dots, \xi(P)]^T$ is a vector of expansion coefficients. A number of possible reduced-rank representations of \mathbf{H}_{eq} will be presented later.

III. JOINT ESTIMATION OF THE UNKNOWN PARAMETERS

We arrange the PSS position, sector ID and IFO into a vector $\boldsymbol{\varphi} = [q, u, \nu]$ and let $\boldsymbol{\eta} = [\boldsymbol{\xi}, \sigma^2, \sigma_w^2]$ be the set of nuisance parameters. The log-likelihood function (LLF) for the unknown quantities $\{\boldsymbol{\varphi}, \boldsymbol{\eta}\}$ is obtained from (3) as

$$\Lambda(\tilde{\boldsymbol{\varphi}}, \tilde{\boldsymbol{\eta}}) = - \sum_{\substack{k=1 \\ k \neq q}}^{N_Q} \left[73 \ln(\pi \tilde{\sigma}_k^2) + \frac{1}{\tilde{\sigma}_k^2} \|\mathbf{X}_k\|^2 \right] \quad (5)$$

$$- 73 \ln(\pi \tilde{\sigma}_w^2) - \frac{1}{\tilde{\sigma}_w^2} \sum_{n=-36}^{36} \left| X_{\tilde{q}}(n) - s(\tilde{\boldsymbol{\varphi}}, \tilde{\boldsymbol{\xi}}; n) \right|^2$$

where we have defined $s(\tilde{\boldsymbol{\varphi}}, \tilde{\boldsymbol{\xi}}; n) = \tilde{H}_{eq}(n - \tilde{\nu})a_{\tilde{u}}(n - \tilde{\nu})$ with $\tilde{H}_{eq} = \mathbf{B}\tilde{\boldsymbol{\xi}}$. The joint ML estimate of the unknown parameters is found by looking for the global maximum of $\Lambda(\tilde{\boldsymbol{\varphi}}, \tilde{\boldsymbol{\eta}})$. Maximizing with respect to $\tilde{\sigma}^2$ and $\tilde{\sigma}_w^2$ produces

$$\hat{\sigma}_k^2 = \frac{1}{73} \|\mathbf{X}_k\|^2 \quad (6)$$

and

$$\hat{\sigma}_w^2 = \frac{1}{73} \sum_{n=-36}^{36} \left| X_{\tilde{q}}(n) - s(\tilde{\boldsymbol{\varphi}}, \tilde{\boldsymbol{\xi}}; n) \right|^2. \quad (7)$$

These results are substituted back into (5) in place of $\tilde{\sigma}_k^2$ and $\tilde{\sigma}_w^2$, yielding

$$\Lambda(\tilde{\boldsymbol{\varphi}}, \tilde{\boldsymbol{\xi}}) = 73 \left[- \sum_{k=1}^{N_Q} \ln \left(\frac{\pi}{73} \|\mathbf{X}_k\|^2 \right) + \ln \left(\frac{\pi}{73} \|\mathbf{X}_{\tilde{q}}\|^2 \right) \right. \quad (8)$$

$$\left. - N_Q - \ln \left(\frac{\pi}{73} \sum_{n=-36}^{36} \left| X_{\tilde{q}}(n) - s(\tilde{\boldsymbol{\varphi}}, \tilde{\boldsymbol{\xi}}; n) \right|^2 \right) \right].$$

Skipping irrelevant multiplicative and additive terms independent of the optimization variables and exploiting the monotonicity of the log function, we may replace $\Lambda(\tilde{\boldsymbol{\varphi}}, \tilde{\boldsymbol{\xi}})$ by the equivalent objective function

$$\Lambda_1(\tilde{\boldsymbol{\varphi}}, \tilde{\boldsymbol{\xi}}) = - \frac{\sum_{n=-36}^{36} \left| X_{\tilde{q}}(n) - \tilde{H}_{eq}(n - \tilde{\nu})a_{\tilde{u}}(n - \tilde{\nu}) \right|^2}{\|\mathbf{X}_{\tilde{q}}\|^2}. \quad (9)$$

To proceed further, we make a change of the indexing variable $n - \tilde{\nu} \rightarrow m$ and recall that the PSS values $a_u(m)$ are non-zero only for $m \in \mathcal{I}$ as specified in (1). Hence, assuming that $|\tilde{\nu}| \leq 5$, after dropping an immaterial term in (9) we obtain

$$\Lambda_2(\tilde{\boldsymbol{\varphi}}, \tilde{\boldsymbol{\xi}}) = \frac{2\Re \left\{ \sum_{m=-31}^{31} Z_{\tilde{q}}(\tilde{u}, \tilde{\nu}; m) \tilde{H}_{eq}^*(m) \right\} - \|\tilde{H}_{eq}\|^2}{\|\mathbf{X}_{\tilde{q}}\|^2}. \quad (10)$$

where we have defined $Z_{\tilde{q}}(\tilde{u}, \tilde{\nu}; m) = X_{\tilde{q}}(m + \tilde{\nu})a_{\tilde{u}}^*(m)$. Denoting by $\mathbf{Z}_{\tilde{q}}(\tilde{u}, \tilde{\nu})$ the 63-dimensional vector with entries $\{Z_{\tilde{q}}(\tilde{u}, \tilde{\nu}; m); |m| \leq 31\}$, we may express $\Lambda_2(\tilde{\boldsymbol{\varphi}}, \tilde{\boldsymbol{\xi}})$ in matrix notation as

$$\Lambda_2(\tilde{\boldsymbol{\varphi}}, \tilde{\boldsymbol{\xi}}) = \frac{2\Re \left\{ \tilde{\boldsymbol{\xi}}^H \mathbf{B}^H \mathbf{Z}_{\tilde{q}}(\tilde{u}, \tilde{\nu}) \right\} - \tilde{\boldsymbol{\xi}}^H \mathbf{B}^H \mathbf{B} \tilde{\boldsymbol{\xi}}}{\|\mathbf{X}_{\tilde{q}}\|^2}. \quad (11)$$

The maximum of $\Lambda_2(\tilde{\boldsymbol{\varphi}}, \tilde{\boldsymbol{\xi}})$ with respect to $\tilde{\boldsymbol{\xi}}$ is achieved at

$$\hat{\boldsymbol{\xi}} = (\mathbf{B}^H \mathbf{B})^{-1} \mathbf{B}^H \mathbf{Z}_{\tilde{q}}(\tilde{u}, \tilde{\nu}) \quad (12)$$

and plugging this result back into (11) yields the concentrated likelihood function

$$\Lambda_3(\tilde{\boldsymbol{\varphi}}) = \frac{\mathbf{Z}_{\tilde{q}}^H(\tilde{u}, \tilde{\nu}) \mathbf{G} \mathbf{Z}_{\tilde{q}}(\tilde{u}, \tilde{\nu})}{\|\mathbf{X}_{\tilde{q}}\|^2} \quad (13)$$

where $\mathbf{G} = \mathbf{B} (\mathbf{B}^H \mathbf{B})^{-1} \mathbf{B}^H$. The joint ML estimate of the unknown parameters is eventually obtained as

$$\hat{\boldsymbol{\varphi}} = \arg \max_{\tilde{\boldsymbol{\varphi}}} \{\Lambda_3(\tilde{\boldsymbol{\varphi}})\} \quad (14)$$

which requires a search over the multi-dimensional domain spanned by $\tilde{\boldsymbol{\varphi}}$. However, since $\tilde{\boldsymbol{\varphi}} = [\tilde{q}, \tilde{u}, \tilde{\nu}]$ has integer-valued entries, there is only a finite number of hypothesized values of $\tilde{\boldsymbol{\varphi}}$. At this stage, the problem arises as how to select a suitable basis $\{\mathbf{b}_1, \mathbf{b}_2, \dots, \mathbf{b}_P\}$ for the reduced-rank representation of \mathbf{H}_{eq} which can exhibit low-sensitivity to the timing error θ . Possible solutions are presented in the next Section.

IV. REDUCED-RANK REPRESENTATION OF THE CHANNEL FREQUENCY RESPONSE

A. Problem formulation

In OFDM systems, the CFR is typically expressed in terms of the discrete-time CIR as

$$H(n) = \sum_{\ell=0}^{L-1} h(\ell) e^{-j2\pi n\ell/N}. \quad (15)$$

Recalling that $H_{eq}(n) = H(n)e^{-j2\pi n\theta/N}$, from (15) it follows that the equivalent CFR takes the form

$$H_{eq}(n) = \sum_{\ell=\theta}^{L+\theta-1} h(\ell - \theta) e^{-j2\pi n\ell/N}. \quad (16)$$

Since coarse timing recovery schemes for OFDM systems adopt a back-off design wherein the timing estimates are pre-advanced to avoid inter-block-interference at the DFT output [22], in the sequel it is assumed that there is no negative timing error. This amounts to letting θ vary in the set $\{0, 1, \dots, \theta_{\max}\}$, where θ_{\max} is selected on the basis of the accuracy of the timing estimator. In such a case, the equivalent CFR can be written in matrix notation as

$$\mathbf{H}_{eq} = \mathbf{F} \mathbf{h}_{eq} \quad (17)$$

where $\mathbf{h}_{eq} = [\mathbf{0}_\theta^T \quad \mathbf{h}^T \quad \mathbf{0}_{\theta_{\max}-\theta}^T]^T$ is the equivalent CIR vector of order $L_{eq} = L + \theta_{\max}$ and \mathbf{F} is a $63 \times L_{eq}$ matrix with entries

$$[\mathbf{F}]_{n,\ell} = e^{-j2\pi n\ell/N} \quad |n| \leq 31, \quad 0 \leq \ell \leq L_{eq} - 1. \quad (18)$$

Since in a practical LTE scenario the normalized timing error may be as large as 40 [16], the channel order L_{eq} is expected to be close or even to exceed the value 63. In this case, we cannot interpret (17) as a reduced-rank representation of \mathbf{H}_{eq} and the goal is to find a basis $\{\mathbf{b}_1, \mathbf{b}_2, \dots, \mathbf{b}_P\}$ of order $P \ll 63$ such that the orthogonal projection of \mathbf{H}_{eq} on the selected basis, say $\mathbf{H}_P = \mathbf{G} \mathbf{H}_{eq}$, is a good approximation of \mathbf{H}_{eq} . The accuracy of such an approximation can be measured in terms of the mean-square-error (MSE) between \mathbf{H}_{eq} and \mathbf{H}_P , which is defined as $E\{\|\mathbf{H}_{eq} - \mathbf{H}_P\|^2\}$. Recalling that $\mathbf{G} = \mathbf{B} (\mathbf{B}^H \mathbf{B})^{-1} \mathbf{B}^H$, from (17) the MSE is found to be

$$\text{MSE}(\mathbf{B}) = E\{\mathbf{h}_{eq}^H \mathbf{F}^H \mathbf{G}^\perp \mathbf{F} \mathbf{h}_{eq}\} \quad (19)$$

where we have taken into account that $\mathbf{G}^\perp = \mathbf{I}_{63} - \mathbf{G}$ is an idempotent matrix and we have explicitly indicated the dependence of the MSE on the expansion matrix \mathbf{B} . After standard manipulations, we can rewrite (19) as

$$\text{MSE}(\mathbf{B}) = \text{tr}\{\mathbf{G}^\perp \mathbf{F} \mathbf{C}_{eq} \mathbf{F}^H\} \quad (20)$$

with $\mathbf{C}_{eq} = E\{\mathbf{h}_{eq} \mathbf{h}_{eq}^H\}$ being the covariance matrix of \mathbf{h}_{eq} .

B. MMSE reduced-rank representation

For a fixed value of P , the optimum expansion basis is the one that minimizes $\text{MSE}(\mathbf{B})$. Neglecting an irrelevant additive term independent of \mathbf{B} , it is seen that the minimum of $\text{MSE}(\mathbf{B})$ is achieved by maximizing the metric

$$\gamma(\mathbf{B}) = \text{tr}\{\mathbf{B} (\mathbf{B}^H \mathbf{B})^{-1} \mathbf{B}^H \mathbf{F} \mathbf{C}_{eq} \mathbf{F}^H\} \quad (21)$$

with respect to \mathbf{B} . To solve this problem, it is convenient to consider the compact singular value decomposition (SVD) of \mathbf{B} , which is given by

$$\mathbf{B} = \mathbf{U} \mathbf{\Sigma} \mathbf{V}^H \quad (22)$$

where $\mathbf{\Sigma} \in \mathbb{R}^{P \times P}$ is the diagonal matrix containing the P non-zero singular values of \mathbf{B} sorted in decreasing order, with the columns of $\mathbf{U} \in \mathbb{C}^{63 \times P}$ and $\mathbf{V} \in \mathbb{C}^{P \times P}$ being the corresponding left and right eigenvectors, respectively. Substituting (22) into (21) and observing that $\mathbf{U}^H \mathbf{U} = \mathbf{V}^H \mathbf{V} = \mathbf{I}_P$, after some algebraic computations we can rewrite $\gamma(\mathbf{B})$ as

$$\gamma(\mathbf{B}) = \text{tr}\{\mathbf{U}^H \mathbf{F} \mathbf{C}_{eq} \mathbf{F}^H \mathbf{U}\} \quad (23)$$

from which we see that the objective function only depends on \mathbf{U} . Maximizing the right-hand-side of (23) with respect to \mathbf{U} is a well-known optimization problem, whose solution is obtained by selecting as columns of \mathbf{U} the P eigenvectors of $\mathbf{F} \mathbf{C}_{eq} \mathbf{F}^H$ associated to the P largest eigenvalues. In the sequel, we denote by \mathbf{U}_{MMSE} the matrix \mathbf{U} provided by such a design criterion. Since $\mathbf{\Sigma}$ and \mathbf{V} can be arbitrarily chosen without affecting the value of the MSE, for simplicity we let $\mathbf{\Sigma} = \mathbf{V} = \mathbf{I}_P$ and obtain $\mathbf{B} = \mathbf{U}_{MMSE}$.

Unfortunately, computing \mathbf{U}_{MMSE} requires knowledge of \mathbf{C}_{eq} , which depends on the channel power delay profile and the timing error. Since these quantities are generally unknown at the receiver, the exact MMSE solution cannot be pursued in practice. A possible way out is found by allowing the system to operate in a mismatched mode wherein \mathbf{C}_{eq} is replaced by $\mathbf{I}_{L_{eq}}$. This leads to an approximated MMSE (AMMSE) solution, say $\mathbf{B} = \mathbf{U}_{AMMSE}$, in which the columns of \mathbf{B} are the P normalized eigenvectors of $\mathbf{F} \mathbf{F}^H$ associated to the P largest eigenvalues. In such a case, the concentrated likelihood function in (13) becomes

$$\Lambda_3(\tilde{\varphi}) = \frac{\|\mathbf{U}_{AMMSE}^H \mathbf{Z}_{\tilde{q}}(\tilde{u}, \tilde{v})\|^2}{\|\mathbf{X}_{\tilde{q}}\|^2}. \quad (24)$$

C. Polynomial-based reduced-rank (PRR) representation

An alternative reduced-rank representation of \mathbf{H}_{eq} can be obtained by approximating the CFR with a $(P-1)$ -order polynomial function as

$$H_{eq}(n) \simeq \sum_{p=1}^P \xi(p) n^{p-1} \quad |n| \leq 31. \quad (25)$$

This amounts to putting $\mathbf{B} = \mathbf{B}_{PRR}$, where \mathbf{B}_{PRR} is a $63 \times P$ matrix with entries

$$[\mathbf{B}_{PRR}]_{n,p} = n^{p-1} \quad |n| \leq 31, \quad 1 \leq p \leq P. \quad (26)$$

D. Piecewise-constant reduced-rank (PCRR) representation

The piecewise-constant reduced-rank representation (PCRR) of the CFR is obtained by arranging the 63 SCH subcarriers into P adjacent subbands and assuming that $H_{eq}(n)$ is approximately constant on each subband. Hence, denoting by K_p the number of subcarriers contained in the p th subband (with $p = 1, 2, \dots, P$), we have

$$H_{eq}(n) \simeq \xi(p) \quad J_{p-1} - 31 \leq n \leq J_p - 32 \quad (27)$$

where

$$J_p = \sum_{m=1}^p K_m \quad 1 \leq p \leq P \quad (28)$$

and $J_0 = 0$. If P is an integer divider of 63, all subbands have the same number of subcarriers $K_p = 63/P$. Otherwise, we let $63 = MP + R$, where $M = \text{int}\{63/P\}$ and $R \in \{1, 2, \dots, P-1\}$ are the quotient and remainder of the integer division $63/P$, respectively. Then, the size of the P subbands are designed such that $K_p = M + 1$ for $1 \leq p \leq R$ and $K_p = M$ for $R + 1 \leq p \leq P$. In matrix notation, \mathbf{H}_{eq} can be written as in (4) after letting $\mathbf{B} = \mathbf{B}_{PCRR}$, where \mathbf{B}_{PCRR} is the $63 \times P$ following matrix

$$\mathbf{B}_{PCRR} = \begin{bmatrix} \mathbf{1}_{K_1} & \mathbf{0}_{K_1} & \cdots & \mathbf{0}_{K_1} \\ \mathbf{0}_{K_2} & \mathbf{1}_{K_2} & \cdots & \mathbf{0}_{K_2} \\ \vdots & \vdots & \ddots & \vdots \\ \mathbf{0}_{K_P} & \mathbf{0}_{K_P} & \cdots & \mathbf{1}_{K_P} \end{bmatrix} \quad (29)$$

In such a case, the concentrated likelihood function in (13) becomes

$$\Lambda_3(\tilde{\varphi}) = \frac{1}{\|\mathbf{X}_{\tilde{q}}\|^2} \sum_{p=1}^P \frac{1}{K_p} \left| \sum_{n=J_{p-1}-31}^{J_p-32} Z_{\tilde{q}}(\tilde{u}, \tilde{\nu}; n) \right|^2 \quad (30)$$

which is reminiscent of the partial correlation method presented in [18]. Interestingly, letting $P = 1$ in (30) yields

$$\Lambda_3(\tilde{\varphi}) = \frac{1}{63 \|\mathbf{X}_{\tilde{q}}\|^2} \left| \sum_{n=-31}^{31} Z_{\tilde{q}}(\tilde{u}, \tilde{\nu}; n) \right|^2 \quad (31)$$

which coincides with the conventional frequency-domain correlation-based (CFDC) metric originally proposed in [14] for the joint estimation of u and ν .

E. Complexity issues

The processing load of the estimator (14) depends on which reduced-rank representation is adopted for the CFR. For both the AMMSE and PRR solutions, the metric $\Lambda_3(\tilde{\varphi})$ can be efficiently computed as

$$\Lambda_3(\tilde{\varphi}) = \frac{\|\mathbf{C}^H \mathbf{B}^H \mathbf{Z}_{\tilde{q}}(\tilde{u}, \tilde{\nu})\|^2}{\|\mathbf{X}_{\tilde{q}}\|^2} \quad (32)$$

where $\mathbf{C}\mathbf{C}^H = (\mathbf{B}^H \mathbf{B})^{-1}$ is the Choleski decomposition of $(\mathbf{B}^H \mathbf{B})^{-1}$, while for the PCRR it is convenient to evaluate $\Lambda_3(\tilde{\varphi})$ as indicated in (30). In any case, for each new received OFDM symbol, the receiver must compute the quantities $\|\mathbf{X}_{\tilde{q}}\|^2$ and $\mathbf{Z}_{\tilde{q}}(\tilde{u}, \tilde{\nu})$. Assuming that the entries of $\mathbf{X}_{\tilde{q}}$ are available, 291 floating-point-operations (flops) are required to get $\|\mathbf{X}_{\tilde{q}}\|^2$, while 372 flops are needed to evaluate $\mathbf{Z}_{\tilde{q}}(\tilde{u}, \tilde{\nu})$ for each couple $(\tilde{u}, \tilde{\nu})$. When using the AMMSE solution, the numerator of $\Lambda_3(\tilde{\varphi})$ in (32) is computed with $498P$ flops for each $(\tilde{u}, \tilde{\nu})$. This figure reduces to $250P$ flops with the PRR approximation as in this case the matrix $\mathbf{C}^H \mathbf{B}^H$ is real-valued. As for the PCRR, evaluating $\Lambda_3(\tilde{\varphi})$ in (30) starting from $\|\mathbf{X}_{\tilde{q}}\|^2$ and $\mathbf{Z}_{\tilde{q}}(\tilde{u}, \tilde{\nu})$ needs $123 + 3P$ flops for each couple $(\tilde{u}, \tilde{\nu})$, which reduces to 126 flops when considering the CFDC. The overall complexity of the investigated schemes

is summarized in Table II for each received OFDM symbol. In writing these figures we have borne in mind that \tilde{u} varies in the set $\{25, 29, 34\}$ and we have denoted by N_{ν} the number of different values of $\tilde{\nu}$.

TABLE II
COMPLEXITY OF THE INVESTIGATED SCHEMES IN TERMS OF NUMBER OF FLOPS FOR EACH OFDM SYMBOL.

Algorithm	Required flops
AMMSE	$291 + 1116N_{\nu} + 1494N_{\nu}P$
PRR	$291 + 1116N_{\nu} + 750N_{\nu}P$
PCRR	$291 + 1485N_{\nu} + 9N_{\nu}P$
CFDC	$291 + 1494N_{\nu}$

V. SIMULATION RESULTS

Computer simulations have been run to assess the performance of the presented PSS detection and IFO recovery schemes using different reduced-rank representations of the CFR. The LTE simulation set-up is chosen according to the 3GPP specifications [6] and is summarized as follows.

A. Simulation model

We consider a 20 MHz LTE communication system with 15 kHz subcarrier spacing. At the receiver side, the baseband signal is sampled with frequency $f_s = 30.72$ MHz and converted in the frequency-domain through a 2048-point DFT unit. To demonstrate the capability of the investigated scheme in a challenging scenario, we adopt the Extended Typical Urban (ETU) channel model characterized by 9 channel taps with maximum excess delay $\tau_{\max} = 5 \mu\text{s}$. The path gains are modeled as statistically independent random variables with zero-mean and Gaussian distribution (Rayleigh fading). A raised-cosine functions with roll-off 0.22 and time-duration of 6 sampling periods is employed for the pulse shaping, which corresponds to an overall CIR of order $L = \text{int}\{f_s \tau_{\max} + 6\} = 160$. Assuming a maximum normalized timing error $\theta_{\max} = 40$ [16], the length of the equivalent CIR vector \mathbf{h}_{eq} is found to be $L + \theta_{\max} = 200$. However, since parameter P (and the system complexity) is expected to increase with the CIR duration, in the design of the AMMSE we use $L_{eq} = 120$, which amounts to reducing the size of matrix \mathbf{F} from 63×200 to 63×120 . This choice is motivated by the fact that in the ETU channel model there is only one multipath component with a path delay greater than $2.3 \mu\text{s}$ which, moreover, collects less than 3% of the average channel power. The value $L_{eq} = 120$ is also compliant with other LTE channel models, such as the Extended Vehicular A (EVA) and Extended Pedestrian A (EPA), which are characterized by a maximum excess delay of $2.51 \mu\text{s}$ and $0.41 \mu\text{s}$, respectively.

Without any loss of generality, we adopt the extended CP transmission mode wherein 6 OFDM symbols are present in each slot. Since the PSS is transmitted every 10 slots, in our simulations we let $N_Q = 60$. The range of CFO values is related to the oscillator instability, while it is only marginally affected by the UE mobility. Hence, assuming that the stability of commercial oscillators for mobile applications is in the order of ± 10 parts-per-million (ppm) at both the transmit and

receive ends, the maximum CFO value is approximately 2.66 subcarrier spacing at the carrier frequency of 2 GHz. Accordingly, the search range for the IFO is $\mathcal{J}_\nu = \{0, \pm 1, \pm 2, \pm 3\}$, which amounts to putting $N_\nu = 7$. Recalling that the PSS is chosen from a set of three possible ZC sequences with root index $u \in \{25, 29, 34\}$, the overall search space for the triplet $\tilde{\varphi} = [\tilde{q}, \tilde{u}, \tilde{\nu}]$ has cardinality $N_\varphi = 3N_q N_\nu = 1260$.

The accuracy of the PSS detection and IFO recovery schemes is measured in terms of the error rate incurred in the estimation of each parameter of interest q, u and ν . As a global performance indicator, we also consider the overall probability of failure $P_f = \Pr\{\hat{\varphi} \neq \varphi\}$.

B. Performance evaluation

Fig. 2 illustrates the quantity $\text{MSE}(\mathbf{B})$ reported in (20) as a function of P for the investigated reduced-rank CFR representations. As expected, the best results are obtained with $\mathbf{B} = \mathbf{U}_{MMSE}$ since this choice minimizes $\text{MSE}(\mathbf{B})$ for a fixed value of P . Compared to the true MMSE solution, the AMMSE is characterized by a higher MSE, even though it largely outperforms both the PRR and PCRR schemes. Although the accuracy of the considered reduced-rank representations steadily improves with P , the probability of failure P_f cannot exhibit a similar behaviour. The reason is that \mathbf{B} has dimension $63 \times P$ and, accordingly, it becomes a square matrix when $P = 63$. In the latter case, $\mathbf{G} = \mathbf{B}(\mathbf{B}^H \mathbf{B})^{-1} \mathbf{B}^H$ reduces to \mathbf{I}_{63} and $\mathbf{G}^\perp = \mathbf{I}_{63} - \mathbf{G}$ is therefore the null matrix. This situation has two consequences. On one hand, from (20) we see that $\text{MSE}(\mathbf{B}) = 0$, thereby justifying the fact that the MSE decreases as P approaches the value 63. On the other hand, substituting $\mathbf{G} = \mathbf{I}_{63}$ into (13) leads to

$$\Lambda_3(\tilde{\varphi}) = \frac{\|\mathbf{Z}_{\tilde{q}}(\tilde{u}, \tilde{\nu})\|^2}{\|\mathbf{X}_{\tilde{q}}\|^2} \quad (33)$$

or, equivalently,

$$\Lambda_3(\tilde{\varphi}) = \frac{\sum_{m=-31}^{31} |X_{\tilde{q}}(m + \tilde{\nu})|^2}{\|\mathbf{X}_{\tilde{q}}\|^2}. \quad (34)$$

This equation indicates that the metric $\Lambda_3(\tilde{\varphi})$ becomes independent of \tilde{u} when $P = 63$, thereby preventing any possibility to recover the sector index. From the above discussion it follows that parameter P must be judiciously designed so as to meet two conflicting requirements. On one hand, it must be large enough to produce a sufficiently accurate reduced-rank representation of the CFR. On the other hand, it must be adequately small since otherwise the estimation problem contains too many unknown quantities which cannot be estimated reliably.

This intuition is corroborated by the results of Fig. 3, where P_f is shown as a function of P . Here, the signal-to-noise ratio (SNR) is fixed at 8 dB and the timing error is $\theta = \theta_{\max} = 40$. As is seen, for each curve there is an optimum value of P which minimizes P_f . Since the minimum is approximately attained at $P = 5$ by all the considered reduced-rank representations, such a value is used in the

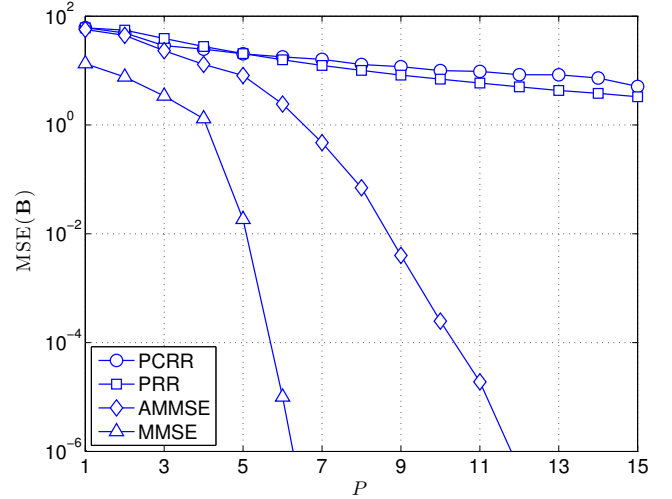


Fig. 2. $\text{MSE}(\mathbf{B})$ vs. P for different reduced-rank CFR representations.

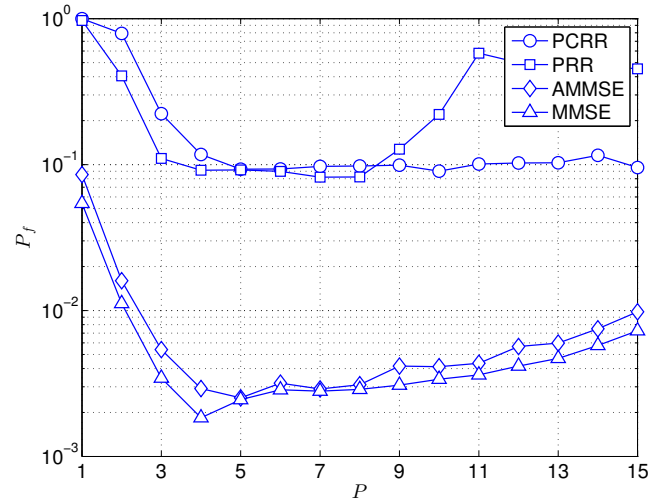


Fig. 3. Probability of synchronization failure vs. P for SNR = 8 dB and $\theta = 40$.

subsequent simulations except for the CFDC scheme, which is obtained from the PCRR by letting $P = 1$.

Fig. 4 illustrates the error rate incurred in detecting the presence of the PSS, say $P_q = \Pr\{\hat{q} \neq q\}$, vs. the SNR for $\theta = 40$. In addition to the investigated schemes, we also consider the PSS differential detector (DD) proposed in [14], which provides an estimate of the unknown parameters $[q, u, \nu]$ by looking for the maximum of the following metric

$$\Lambda_{DD}(\tilde{\varphi}) = \frac{\Re \left\{ \sum_{n=-30}^{31} Z_{\tilde{q}}(\tilde{u}, \tilde{\nu}; n) Z_{\tilde{q}}^*(\tilde{u}, \tilde{\nu}; n-1) \right\}}{\|\mathbf{X}_{\tilde{q}}\|^2} \quad (35)$$

in which the quantities $Z_{\tilde{q}}(\tilde{u}, \tilde{\nu}; n)$ and $Z_{\tilde{q}}^*(\tilde{u}, \tilde{\nu}; n-1)$ obtained from two adjacent frequency bins are multiplied in order to mitigate the impact of the timing error and channel selectivity on the system performance. As expected, AMMSE outperforms all the other methods and achieves a gain of approximately 2 dB over the DD, which further increases to

2.5 dB and 3 dB with respect to PCRR and PRR, respectively. Due to its high sensitivity to timing errors and channel distortions, the CFDC does not work properly in such adverse scenario, and exhibits an error rate which is close to one at all SNR values.

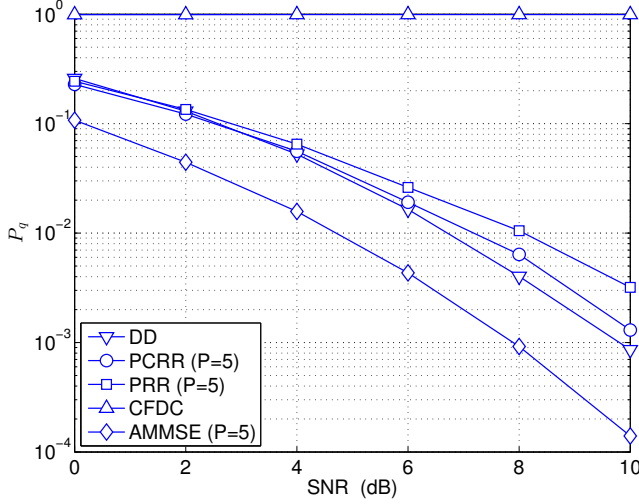


Fig. 4. Error rate incurred in the detection of the PSS vs. SNR for $\theta = 40$.

Figs. 5 and 6 show the error rate incurred in the estimation of the sector index and IFO, respectively, say $P_u = \Pr\{\hat{u} \neq u\}$ and $P_\nu = \Pr\{\hat{\nu} \neq \nu\}$. The operating scenario is the same as that in Fig. 4 and also the trend of the curves is similar, with AMMSE outperforming the other schemes. It is worth noting that the use of AMMSE is more advantageous for the estimation of the IFO than for the other two parameters q and u .

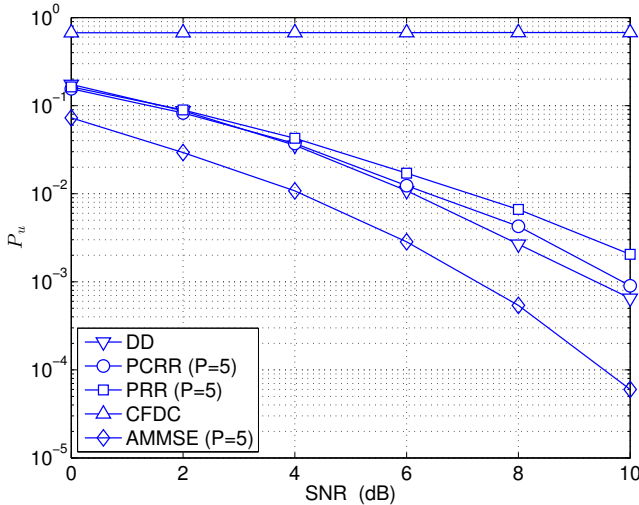


Fig. 5. Error rate incurred in the detection of the sector index u vs. SNR for $\theta = 40$.

The overall system performance is summarized in Fig. 7, where P_f is shown as a function of the SNR with the timing error being fixed to $\theta = 40$. These measurements validate the results of Figs. 4-6 and clearly indicate the superiority of

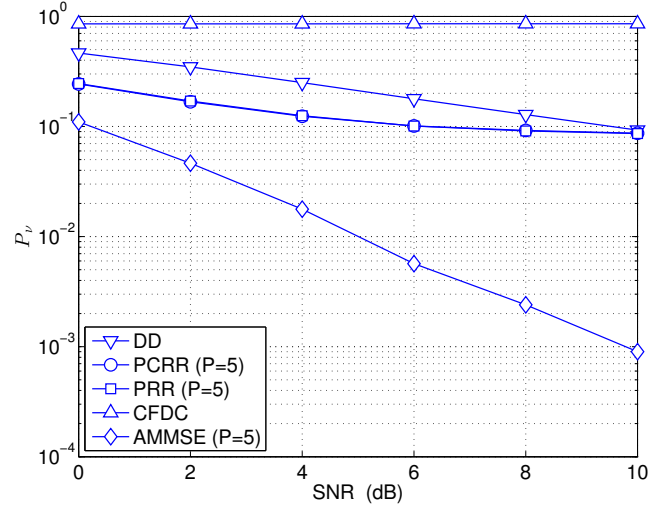


Fig. 6. Error rate incurred in the detection of the IFO ν vs. SNR for $\theta = 40$.

AMMSE over the other methods. In particular, at SNR=10 dB we see that the probability of failure of AMMSE is 10^{-3} , while it increases to 10^{-1} with PCRR, PRR and DD.

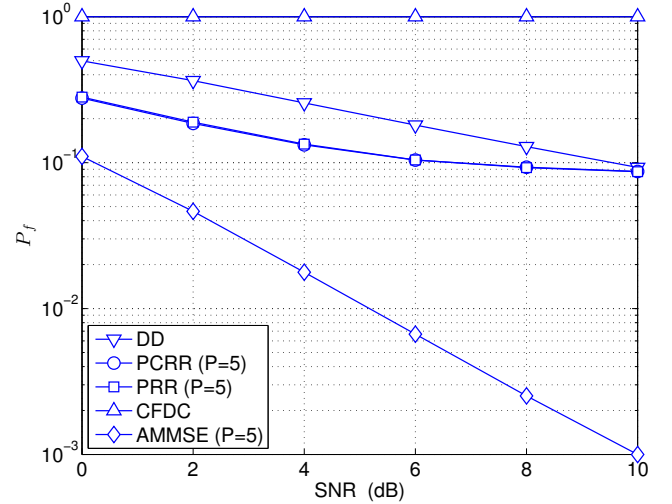


Fig. 7. Probability of synchronization failure vs. SNR for $\theta = 40$.

Fig. 8 illustrates P_f as a function of θ when the SNR is fixed to 8 dB. These results are useful to assess the sensitivity of the considered schemes to residual timing errors and demonstrate the remarkable robustness of both DD and AMMSE to such an impairment. In contrast, the probability of failure of PCRR, PRR and CFDC rapidly deteriorates as θ increases. This is particularly evident for the CFDC, which cannot be used when the timing error exceeds a few sampling periods.

C. Complexity comparison

We conclude our study by comparing the investigated schemes in terms of their computational complexity. From the results reported in Table II it turns out that, in the considered scenario with $N_\nu = 7$ and $P = 5$, the number of

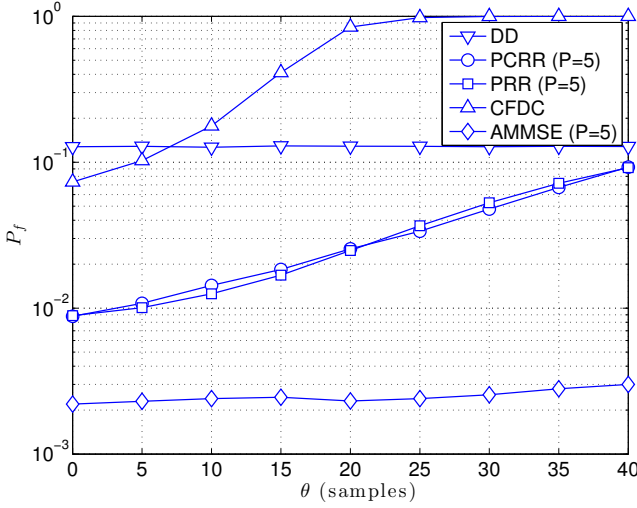


Fig. 8. Probability of synchronization failure vs. θ for SNR = 8 dB.

required kiloflops (kflops) for each received OFDM symbol is approximately 60 for the AMMSE method, 34 for PRR and 11 for both PCRR and CFDC. As for the DD scheme, computing the numerator of $\Lambda_{DD}(\tilde{\varphi})$ in (35) starting from $\mathbf{Z}_{\tilde{q}}(\tilde{u}, \tilde{v})$ needs 245 flops for each couple (\tilde{u}, \tilde{v}) which, after including the computational burden required to get the quantities $\|\mathbf{X}_{\tilde{q}}\|^2$ and $\mathbf{Z}_{\tilde{q}}(\tilde{u}, \tilde{v})$, leads to an overall processing requirement of 13 kflops. These figures indicate that the improved accuracy of the AMMSE is achieved at the price of a higher system complexity. In particular, the number of flops is increased by a factor of two with respect to PCRR, and by a factor 5.5 with respect to the other methods. However, considering the fact that in the investigated simulation set-up the AMMSE is the only scheme that can ensure acceptable error rate performance, the penalty in terms of computational load seems tolerable.

VI. CONCLUSIONS

We have presented an ML approach for joint PSS detection, sector index identification and IFO recovery in the downlink of an LTE system. The proposed scheme (AMMSE) operates in the frequency-domain and is based on a novel MMSE reduced-rank representation of the channel frequency response over the SCH subcarriers, which mitigates the impact of multipath distortions and residual timing errors on the system performance. Compared to existing schemes available in the literature, our method exhibits improved accuracy at the price of a higher computational complexity. The penalty in terms of required flops is justified by the fact that AMMSE can be used in a harsh environment characterized by prolonged delay spreads and non-negligible timing errors, where other competing schemes provide unacceptable performance. Furthermore, it represents a promising candidate for future heterogeneous networks in which the coexistence of femto-, pico- and macro-cells will require fast and successful detection of neighboring cells for efficient interference management and fast handover operations.

REFERENCES

- [1] E. Dahlman, S. Parkvall, J. Sköld, and P. Beming, *3G Evolution: HSPA and LTE for mobile broadband*, Academic Press Inc., 2008.
- [2] 3GPP TS 36.101 v8.9.0 3rd Generation Partnership Project; technical specification group radio access network; evolved universal terrestrial radio access (E-UTRA); user equipment (UE) radio transmission and reception (release 8), Techn. Rep., Dec. 2009.
- [3] H. G. Myung and D. J. Goodman, *Single Carrier FDMA - A new air interface for long term evolution*, New York: John Wiley and Sons, 2008.
- [4] E. W. Yi-Pin and O. Tony, "Cell search in W-CDMA", *IEEE J. Sel. Areas Commun.*, vol. 18, n. 8, pp.1470-1482, Aug. 2000.
- [5] M. M. Wang, A. Agrawal, A. Khandekar, and S. Aedudodla, "Preamble design, system acquisition, and determination in modern OFDMA cellular communications: an overview", *IEEE Commun. Mag.*, vol. 49, n. 7, pp. 164-175, July 2011.
- [6] 3GPP TS 36.211 V8.7.0, "Physical channels and modulation", 2009.
- [7] Y. Tsai, G. Zhang, D. Grieco, F. Ozluturk, and X. Wang, "Cell search in 3GPP long term evolution systems", *IEEE Veh. Technol. Mag.*, pp. 23-29, June 2007.
- [8] M. Sandell, J. J. van de Beek, and P. O. Börjesson, "ML estimation of time and frequency offset in OFDM systems", *IEEE Trans. on Signal Processing*, vol. 45, n. 7, pp.1800-1805, July 1997.
- [9] H. Setiawan and H. Ochi, "A low complexity physical-layer identity detection for 3GPP Long Term Evolution", in *Proc. of the 12th Int. Conf. on Advanced Commun. Techn. (ICACT) 2010*.
- [10] B. M. Popovic and F. Berggren, "Primary synchronization signal in E-UTRA", in *Proc. of 10th Int. Symp. on Spread Spectrum Techn. and Appl. (ISSSTA) 2008*, pp. 426-430, 2008.
- [11] Y. Yu and Q. Zhu, "A novel time synchronization for 3 GPP LTE cell search", in *Proc. of 8th Int. Conf. on Commun. and Net. in China*, 2013.
- [12] Z. Zhang, J. Liu, and K. Long, "Low-complexity cell search with fast PSS identification in LTE", *IEEE Trans. on Vehic. Technology*, vol. 61, n. 4, pp. 1719-1729, May 2012.
- [13] Y. Gao, G. Zhu, X. Chen, D. Wu, and B. Ban, "A modified algorithm of synchronization signal detection for LTE initial cell search", in *Proc. of 6th Int. Conf. on Commun. and Net. in China*, 2011.
- [14] K. Manolakis, D. M. G. Estévez, V. Jungnickel, W. Xu, and C. Drewes, "A closed concept for synchronization and cell search in 3GPP LTE systems", in *Proc. of Wireless Commun. and Net. Conf. (WCNC) 2009*, Budapest, Apr. 2009.
- [15] Y. H. Tsai and T. H. Sang, "A new timing synchronization and cell search procedure resistant to carrier frequency offsets for 3GPP-LTE downlink", in *Proc. of 1st IEEE Int. Conf. on Commun. in China*, pp. 334-338, 2012.
- [16] S. L. Su, Y. C. Lin, and Y. J. Fan, "Joint sector identity and integer part of carrier frequency offset detection by phase-difference in Long Term Evolution cell search process", *IET Communications*, vol. 7, n. 10, pp. 950-959, 2013.
- [17] A. R. Elsherif and M. M. Khairy, "Adaptive primary synchronization signal detection for 3GPP Long Term Evolution", in *Proc. of 9th Int. Wireless Commun. and Mobile Comp. Conf.*, 2013.
- [18] L.-C. Wung, Y.-C. Lin, Y.-J. Fan, and S.-L. Su, "A robust scheme in downlink synchronization and initial cell search for 3GPP LTE systems", in *Proc. of 6th Int. Symp. on Wireless and Pervasive Computing (ISWPC) 2011*, pp. 1-6, 2011.
- [19] M. Morelli and M. Moretti, "ML estimation of timing, integer frequency and primary sequence index in LTE systems", in *Proc. of Int. Conf. on Commun. (ICC)*, 2015.
- [20] M. Morelli and M. Moretti, "Carrier Frequency Offset Estimation for OFDM Direct-Conversion Receivers," *IEEE Trans. Wireless Commun.*, vol.11, no.7, pp. 2670-2679, July 2012.
- [21] B. M. Popovic, "Generalized chirp-like polyphase sequences with optimum correlation properties", *IEEE Trans. Inf. Theory*, vol. 30, n. 3, pp. 769-777, July 1992.
- [22] H. Minn, V. K. Bhargava, and K. B. Letaief, "A robust timing and frequency synchronization for OFDM systems", *IEEE Trans. Wireless Commun.*, vol. 2, n. 4, pp. 822-839, July 2003.
- [23] P. Y. Tsai and H. W. Chang, "A new cell search scheme in 3GPP Long Term Evolution downlink OFDMA systems", in *Proc. of 12th Int. Conf. on Wireless Commun. and Signal Proc.*, 2009.
- [24] X. Yang, Y. Xiong, G. Jia, W. Fang, and X. Zheng, "PSS based time synchronization for 3GPP LTE downlink receivers", in *Proc. of 13th Int. Conf. on Commun. Techn. (ICCT) 2011*, pp. 930-933, 2011.
- [25] C. Y. Chu, I. W. Lai, Y. Y. Lan, and T. D. Chiueh, "Efficient sequential integer CFO and sector identity detection for LTE cell search", *IEEE Wireless Commun. Letters*, vol. 3, n. 4, pp. 389-392, Aug. 2014.

- [26] Y. Shen, T. Luo, and M. Z. Win, "Neighboring cell search for LTE systems", *IEEE Trans. on Wireless Commun.*, vol. 11, n. 3, pp. 908-919, March 2012.
- [27] I. T. S. Sesia and M. Baker, *LTE - the UMTS Long Term Evolution: from theory to practice*, New York: John Wiley and Sons, 2009.